Title
CREEP-SINTERING OF ZINC OXIDE

Authors
Rahaman, M.N.
Jonghe, L.C. De

Publication Date
1986-12-01

LBL-22706
Preprint

Lawrence Berkeley Laboratory
UNIVERSITY OF CALIFORNIA

Materials & Molecular Research Division

Submitted to Journal of Materials Science

CREEP-SINTERING OF ZINC OXIDE

M.N. Rahaman and L.C. De Jonghe

December 1986

Prepared for the U.S. Department of Energy under Contract DE-AC03-76SF00098

DISCLAIMER

CREEP-SINTERING OF ZINC OXIDE

M. N. Rahaman* and L. C. De Jonghe
Materials and Molecular Research Division
Lawrence Berkeley Laboratory
University of California
Berkeley, CA 94720

Abstract

The simultaneous creep and densification of ZnO powder compacts was studied, using a loading dilatometer, at 725°C subjected to uniaxial stresses of up to 0.25 MPa. Between relative densities of 0.50 and 0.85, the dependence of the uniaxial creep rate on density can be described in terms of a stress intensification factor, ϕ, of the form $\phi \sim \exp(aP)$, where a is constant equal to 5.0 and P is the porosity. Comparison of the creep and densification rates showed that the ratio of the linear densification rate to the creep rate is nearly constant over a density range between 0.55 and 0.85, and permitted the evaluation of the sintering stress, which is found to decrease with increasing density. The results are compared with those obtained earlier for CdO and a soda-lime glass powder.

*Present address: University of Missouri-Rolla,
Ceramic Engineering Department,
Rolla, MO 65401

This work was supported by the Division of Materials Sciences, Office of Basic Energy Sciences, U.S. Department of Energy, under Contract No. DE-AC03-76SF00098.

I. INTRODUCTION

It is now widely recognized that heterogeneities (e.g. hard agglomerates, particle or fiber inclusions) present in a powder compact lead to non-uniform local sintering rates which, in turn, produce transient stresses [1-4]. Unless these stresses are relieved by creep processes, they can lead to a reduction in densification rates, and may even cause microcracking in the sintering compact. Clearly, a fundamental parameter for a powder system is the relative magnitude of the densification rate to the creep rate.

The technique of loading dilatometry [5] was developed by the present authors to quantify the interaction between creep and densification during sintering. Basically, a controlled, measured uniaxial stress is applied to the sintering compact. For applied stresses much less than the sintering stress or for creep strains much smaller than the linear densification strain, creep and densification can be treated as independent processes, as found in earlier work on CdO [6,7]. When the applied stresses are comparable to the sintering stress, or the creep strains are comparable to the linear densification strain, as in the case of glass (8,9), there is considerable interaction between the creep and densification processes. The creep rate and the densification rate are then functions of both the applied stress and the sintering stress.

Earlier papers by the present authors using CdO [6,7] explored the usefulness of the loading dilatometer technique and the analysis of the experimental data to evaluate the functional dependence of the stress intensity fiction factor, ϕ, [10-13] and the sintering stress, Σ, [14,15], on density and grain size. Experiments have also been performed on magnesium oxide [16] and soda-lime glass powder [8,9]. The only other published work on the effect of uniaxial (or shear) stress on densification has been performed by Venkatachari and Raj [17] on alumina doped with about 0.25 w% magnesium oxide. Venkatachari and Raj used stresses greater than the sintering stress. Although the creep strains ranged up to $\sim$0.7 while the linear densification strain was less than $\sim$0.15, their results indicated that creep and densification could still be treated as independent processes.

This paper reports on the simultaneous creep and densification behaviour of ZnO powder compacts. The results will be compared with those obtained earlier for CdO and a soda-lime glass powder. The results of these creep-sintering experiments are not only important for the understanding of fundamental issues in the sintering of single phase systems but are also of considerable value in accounting for the densification of heterogeneous powder compacts [16] and particulate composites [3, 18, 19].

II. EXPERIMENTAL

Zinc oxide powder* compacts (6mm diameter by 6 mm), having a green relative density of 0.45±0.01 were made by uniaxial compaction of the powder at ∿20 MPa in a tungsten carbide die. The average grain size of the powder was ∿0.4 m. The compacts were sintered in flowing, dry air ($50 cm^3\ min^{-1}$) for 2 hours in a loading dilatometer. The instrument and its associated control and monitoring equipment have been described in detail elsewhere [5,6]. Sintering was performed at 725°C and under low, uniaxial stresses between 0 and 0.25 MPa. The sintering procedure was similar to that described earlier for CdO [6]. The mass and dimensions of the samples were measured before and after sintering and the final density measured using Archimedes' principle. In a separate set of experiments, sintering was terminated after times between 0 and 2 hours, and the dimensions of these compacts measured using a micrometer.

The average grain sizes of three separate specimens were measured after sintering for 20, 60 and 120 min. Measurements were taken from scanning electron micrographs of polished and thermally etched samples. Samples were vacuum impregnated with epoxy resin and then polished using diamond paste and non-aqueous lubricants. A 'flash-etching' method was used in order to minimize grain growth during the etching stage. Samples were first thermally equilibrated at 500° C, then rapidly inserted into the hot zone of the furnace at 1000°C, and kept

* Reagent grade, Mallinckrodt Inc., Paris Kentucky.

there for 30 sec, after which time they were rapidly removed. This technique produced a light etch that was adequate for delineating the grain boundaries. Grain sizes were measured by counting the number of grains traversed by straight lines of known length. The average grain size was taken as 1.5 times the average intercept length. Dihedral angles were obtained from micrographs of polished samples having a relative density of ~ 0.85.

III. RESULTS

Figure 1 shows the axial shrinkage, $\Delta L/L_0$, versus time, t, for applied loads between 0 and 7N (L_0 = initial sample length and $\Delta L = L - L_0$, where L = instantaneous sample length). A load of 1N represents a stress of 35 kPa on the green, unsintered compact, and t = 0 represents the beginning of shrinkage. The sintering temperature (725°C) was reached after t = 6 min. Each curve is the average of two runs under the same conditions, and each is reproducible to within $\pm 2\%$. Weight losses in the samples were less than 1% after 2 hours at the sintering temperature, and the applied loads could be maintained to within $\pm 5\%$ for the duration of the experiment. It is seen that at any time, t, the axial shrinkage increases with increasing load.

The application of a uniaxial load causes anisotropic shrinkage of the compact, as shown in Fig. 2, where $\Delta L/L_0$ is plotted versus the radial shrinkage $\Delta D/D_0$ (D_0 = initial sample diameter, and $\Delta D = D - D_0$, where D = instantaneous sample diameter). The $\Delta L/L_0$ values are

approximately proportional to $\Delta D/D_0$ and the slopes of the lines increase with increasing load.

The creep strain, ε, was separated from the volumetric densification strain using the results of Figures 1 and 2 and the methodology described by Raj [20]. Figure 3 shows the relative density, ρ, versus log t for zero applied load and for the maximum applied load of 7N. The curves for the other loads have been omitted for clarity. Similar to the results obtained for CdO [6,7], the small loads cause almost no change in ρ. The effect of applied load on the creep behaviour is shown in Fig. 4. It is seen that although ε increases with applied load, the creep strains are small (< 3%). Creep strains of this magnitude are expected to have no effect on the evolution of the pore morphology during creep-sintering. Contributions to the creep strain from anisotropic densification as found in experiments on glass powder [8,9], are therefore expected to be absent in these experiments on ZnO.

The relative densification rate, $\dot{\rho}$, and the creep rate, $\dot{\varepsilon}$, were obtained as a function of ρ (or t) by fitting smooth curves to the results of Figures 3 and 4 and differentiating. However, to evaluate the results at constant applied stress, a small correction has to be made for the change in the cross-sectional area of the sample during the experiment, as outlined earlier [7].

Figure 5 shows the results for $\dot{\rho}$ and $\dot{\varepsilon}$ versus ρ at constant applied stresses. The curves for $\dot{\rho}$ and $\dot{\varepsilon}$ have similar shapes and decrease approximately linearly with ρ for values of ρ between 0.5 and 0.8. Similar trends were obtained earlier for CdO [7]. The results for $\dot{\varepsilon}$ versus the applied stress, σ_a, for relative densities between 0.6 and 0.8 are shown in Fig. 6. A linear dependence of $\dot{\varepsilon}$ on σ_a is found, and this indicates a diffusion mechanism for the creep process. The small negative intercept for $\dot{\varepsilon}$ for $\sigma_a = 0$ is due to a small amount of anisotropic densification in the die-pressed compact, i.e. for the sample sintered under no load, the radial shrinkage is slightly greater than the axial shrinkage.

Figure 7 shows scanning electron micrographs of polished and etched samples sintered for 20 min and 120 min. Grain growth is relatively small and the initial grain size of the compact increases by a factor of $\sim$2 after sintering for 2 hours. The increase in the grain size can be best fitted to a cubic growth law, Fig. 8, of the form $(G/G_o)^3 = 1 + kt$, where k is a constant equal to 0.05 and G_o is the initial grain size. The mean value of the dihedral angle was 118$\pm$10 degrees.

IV. DISCUSSION

(1) The Stress Intensification Factor, ϕ.

As outlined earlier [7], the creep data may be treated in terms of a general equation of the form

$$\dot{\varepsilon} = \frac{CD\Omega\sigma_e^p}{GX_o^{m-1} k_B T} \qquad (1)$$

where X_0 is the radius of a load-bearing grain boundary area between two grains, or the pore spacing, C is a constant defined by the geometry, D is the diffusivity, Ω is the molecular volume, k_B is the Boltzmann constant, T is the absolute temperature, σ_e is the effective mean stress on the load-bearing parts of grain boundaries, and m and n are exponents characteristic of the creep mechanism. For diffusion-controlled creep p = 1, as observed here for ZnO. For lattice diffusion (Nabarro-Herring creep [21, 22], m = 2, while for grain boundary diffusion (Coble creep [23]), m = 3. According to Gupta and Coble [24], mass transport during sintering of ZnO occurs by lattice diffusion. For the low stresses used in these experiments the creep mechanism is expected to be similar to that for densification, so that m = 2. The stress intensification factor, ϕ, is defined as

$$\phi = (A/A_e) = (G/X_0)^2 \tag{2}$$

where A_e and A are the effective, load-bearing area and the total cross-sectional area respectively. For ZnO, equation (1) may then be simplified to give

$$G^2\dot{\varepsilon} = K_1\sigma_a\phi^{3/2} \tag{3}$$

where K_1 is a constant at a fixed temperature. A plot of $G^2\dot{\varepsilon}$ versus ρ, as shown in Fig. 9, would then give the functional dependence of ϕ on σ. It is seen that ϕ is an exponential function of ρ for values of ρ between 0.55 and 0.85, i.e. $\phi = \exp(aP)$, where a = 5.0 and P the porosity ($P = 1-\rho$). The observed value of a is somewhat lower than the value a = 6 predicted by the Beere model [11-13] for the observed dihedral angle of ~120 degrees. For CdO [7], with almost the same dihedral angle (125 degrees), it was observed that a = 2.0.

Thus for both CdO and ZnO, the observed dependence of ϕ on porosity is stronger than that of the Coble expression [3] of $\phi \sim 1/\rho$, but significantly weaker than that predicted by the Beere model [11, 12]. As pointed out by Vieira and Brook [13], the Coble expression may be more valid for $\rho < 0.9$, i.e. for the final stage of densification when the pores are isolated, and nearly spherical. The observed deviation from the Beere model may originate from at least two main assumptions of the theory; first, that rapid surface relaxation occurs to produce equilibrium pore shapes, and second, that the number of pores per grain remains constant. The first assumption cannot, at present, be tested due to the lack of surface diffusion coefficients for CdO and ZnO, but the second is not completely valid since grain growth and pore size distributions can lead to a reduction in the average number of pores per grain.

(2) The Ration of Densification Rate to Creep Rate

As outlined earlier, the ratio of the densification rate to the creep rate is of fundamental importance in the understanding of the sintering behaviour of composites and other heterogeneous systems. Figure 10 shows the ratio of the linear densification rate to the creep rate, $\dot{\rho}/3\rho\dot{\varepsilon}$, versus ρ. This ratio was evaluated at a constant applied stress of 0.25 MPa.

It is seen that $\dot{\rho}/3\rho\dot{\varepsilon}$ is approximately constant over density range between 0.55 and 0.85. This ratio has also been found to be nearly constant with density for CdO and a soda-lime glass powder [25].

(3) The Sintering Stress, Σ.

Following equation (3), the expression for the densification rate may be written as

$$G^2\dot{\rho} = K_2\Sigma\phi^{1/2} \tag{4}$$

where K_2 is a constant, Σ is the sintering stress and the densificaiton mechanism is lattice diffusion. Then from equations (3) and (4)

$$(\dot{\rho}/3\rho\dot{\varepsilon}) = (K_1/K_2)\Sigma/(\sigma_a\phi) = K_3\Sigma/(\sigma_a\phi) \tag{5}$$

where K_3 is a constant. Since $(\dot{\rho}/3\rho\dot{\varepsilon})$ has been observed to be relatively constant, then the most significant dependence of Σ on microstructural parameters is contained in the term ϕ [25]. For creep and densification by lattice diffusion, transport of matter occurs from grain boundaries under compression and grain boundaries under tension to adjacent pores. The constants K_1 and K_2 in equation (5) can then be considered to be approximately equal so that

$$\Sigma = \left(\frac{\dot{\rho}}{3\rho\dot{\varepsilon}}\right)\sigma_a\phi \tag{6}$$

The magnitude of the sintering stress can then be found from equation (6), and is shown in Fig. 11 as a function of ρ. The value of Σ decreases from $\sim$20 MPa at $\rho = 0.55$ to $\sim$5 MPa at $\rho = 0.85$. Since the grain size, G, increases by a factor of ≤ 2 over this density range, the decrease in Σ cannot be explained entirely in terms of grain growth and pore growth. Other factors contributing to the decrease in Σ during sintering are, at present, not clearly identified but may be related to the changing pore morphology and pore size distributions.

V. CONCLUSIONS

The loading dilatometer technique has been used to study the simultaneous creep and densification behaviour of ZnO powder compacts and the results were compared with those obtained earlier for an oxide ceramic, CdO, and a glass. The general trends in the results were similar to those for CdO but some important differences were observed.

The stress intensification factor, ϕ, was found to have an exponential dependence on porosity, P, of the form $\phi \sim \exp(aP)$, where a is a constant equal to 5. Although this expression is functionally similar to that for CdO, it showed a stronger dependence on porosity for approximately the same dihedral angle.

The sintering stress, Σ, was found to decrease with increasing density, but this decrease cannot be entirely explained by grain growth and pore growth during sintering.

The ratio of the linear densification rate to the creep rate was nearly constant over a wide range of density between 0.55 and 0.85. Similar behaviour has been observed for CdO and glass, although the actual magnitude of this ratio varied significantly for the different materials.

Acknowledgment: This work was supported by the Division of Materials Sciences, Office of Basic Energy Sciences, U.S. Department of Energy, under Contract No. DE-AC03-76SF00098.

REFERENCES

1. A. G. Evans, J. Am. Ceram. Soc., 65 (1982) 497

2. R. Raj and R. K. Bordia, Acta Metall., 32 (1984) 1003.

3. L. C. De Jonghe, M. N. Rahaman, and C-H. Hsueh, Acta Metall., 34 (1986) 1467.

4. C-H. Hsueh, A. G. Evans and R. M. McMeeking, J. Am. Ceram. Soc., 69 (1986) C-64.

5. L. C. De Jonghe and M. N. Rahaman, Rev. Sci. Instrum., 55 (1984) 2010.

6. M. N. Rahaman and L. C. De Jonghe, J. Am. Ceram. Soc., 67 (1984) C-205.

7. M. N. Rahaman, L. C. De Jonghe, and R. J. Brook, J. Am. Ceram. Soc., 69 (1986) 53.

8. M. N. Rahaman and L. C. De Jonghe, LBL Report 20713, December 1985, submitted to J. Am. Ceram. Soc.

9. M. N. Rahaman, L. C. De Jonghe, and R. J. Brook, LBL Report 20714, December 1985, submitted to J. Am. Ceram. Soc.

10. R. L. Coble, J. Appl. Phys., 41 (1970) 4798.

11. W. Beere, Acta Metall., 23 (1975) 131.

12. W. Beere, Acta Metall., 23 (1975) 139.

13. J. M. Vieira and R. J. Brook, J. Am. Ceram. Soc., 67 (1984) 245.

14. R. A. Gregg and F. N. Rhines, Metall. Trans., 4 (1973) 1365.

15. E. H. Aigeltinger, Int. J. Powder Metall. Powder Technol., 11 (1975) 195.

16. M. Lin, M. N. Rahaman, and L. C. De Jonghe, LBL Report 21508, May 1986, submitted to J. Am. Ceram. Soc.

17. K. R. Venkatachari and R. Raj, J. Am. Ceram. Soc., 69 (1986) 499.

18. R. K. Bordia and R. Raj, J. Am. Ceram. Soc. 69 (1986) C-55.

19. M. N. Rahaman and L. C. De Jonghe, Unpublished work.

20. R. Raj, J. Am. Ceram. Soc., 65 (1982) C-46.

21. F. R. N. Nabarro, in Report on the Conference on Strength of Solids (Bristol 1947, 1948) p. 75.

22. C. Herring, J. Appl. Phys., 21 (1950) 437.

23. R. L. Coble, J. Appl. Phys., 34 (1963) 1679.

24. T. K. Gupta and R. L. Coble, J. Am. Ceram. Soc., 51 (1968) 521.

25. L. C. De Jonghe and M. N. Rahaman, Submitted to Acta. Metall.

LIST OF FIGURES

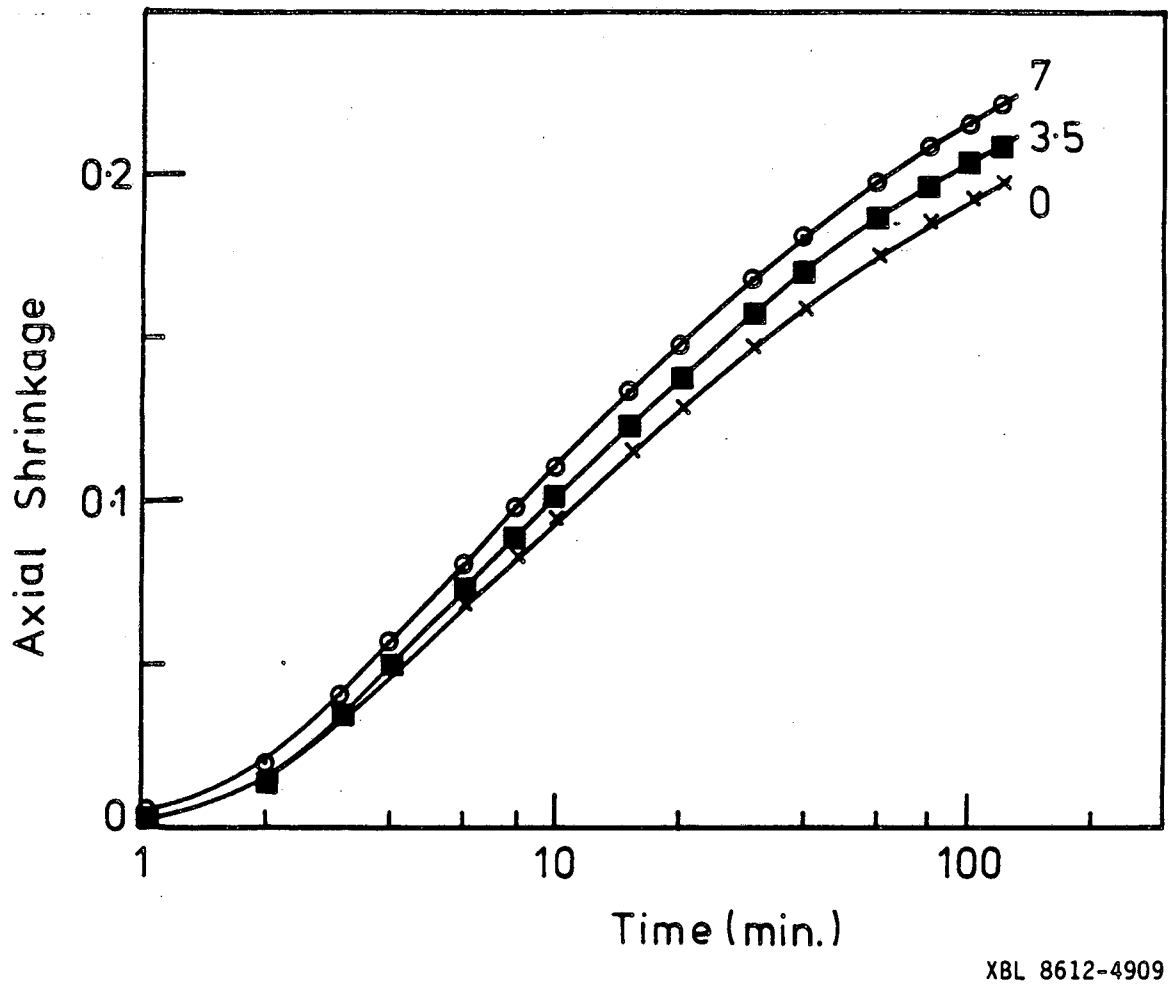

Fig. 1

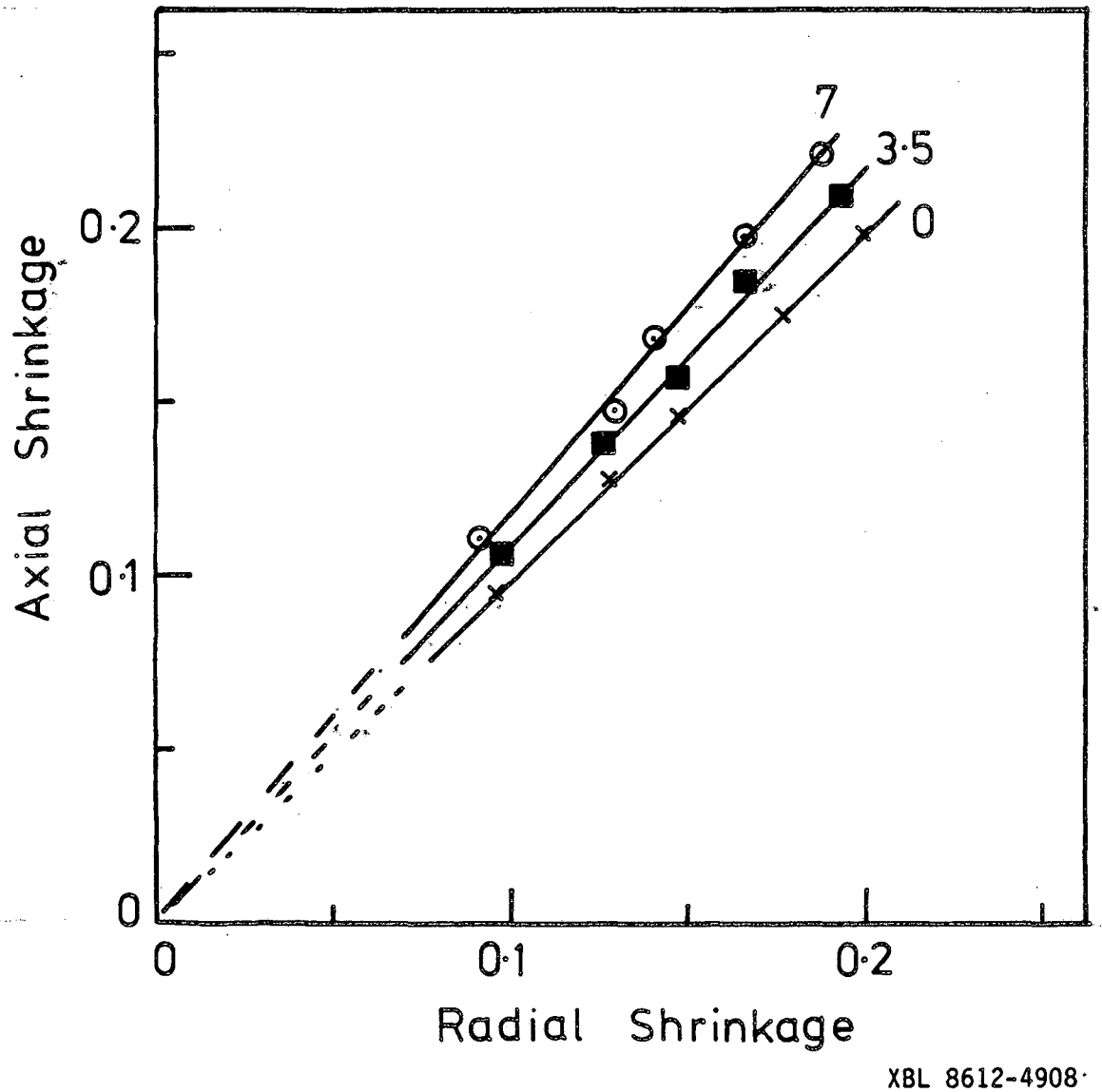

XBL 8612-4908

Fig. 2.

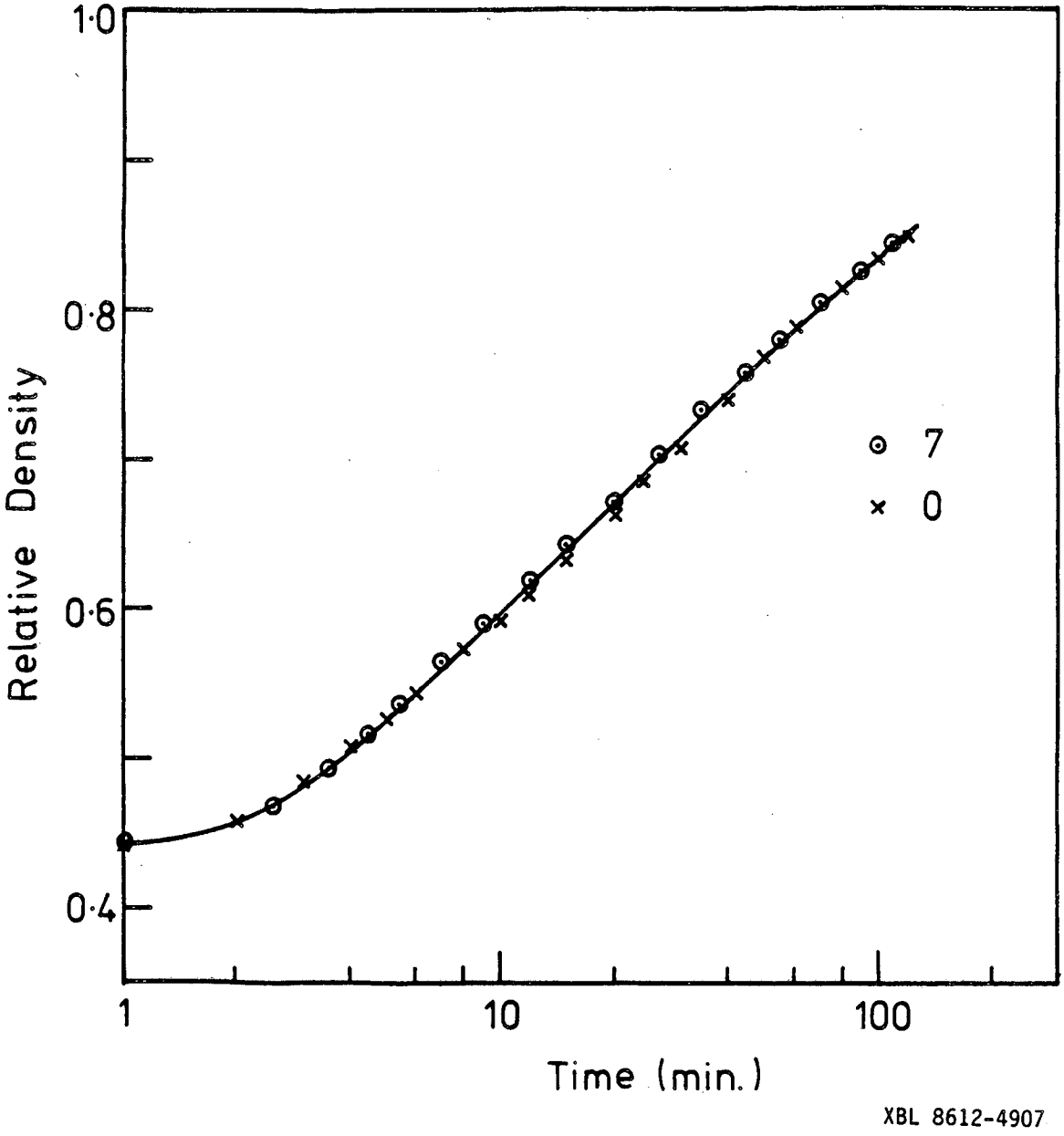

Fig. 3

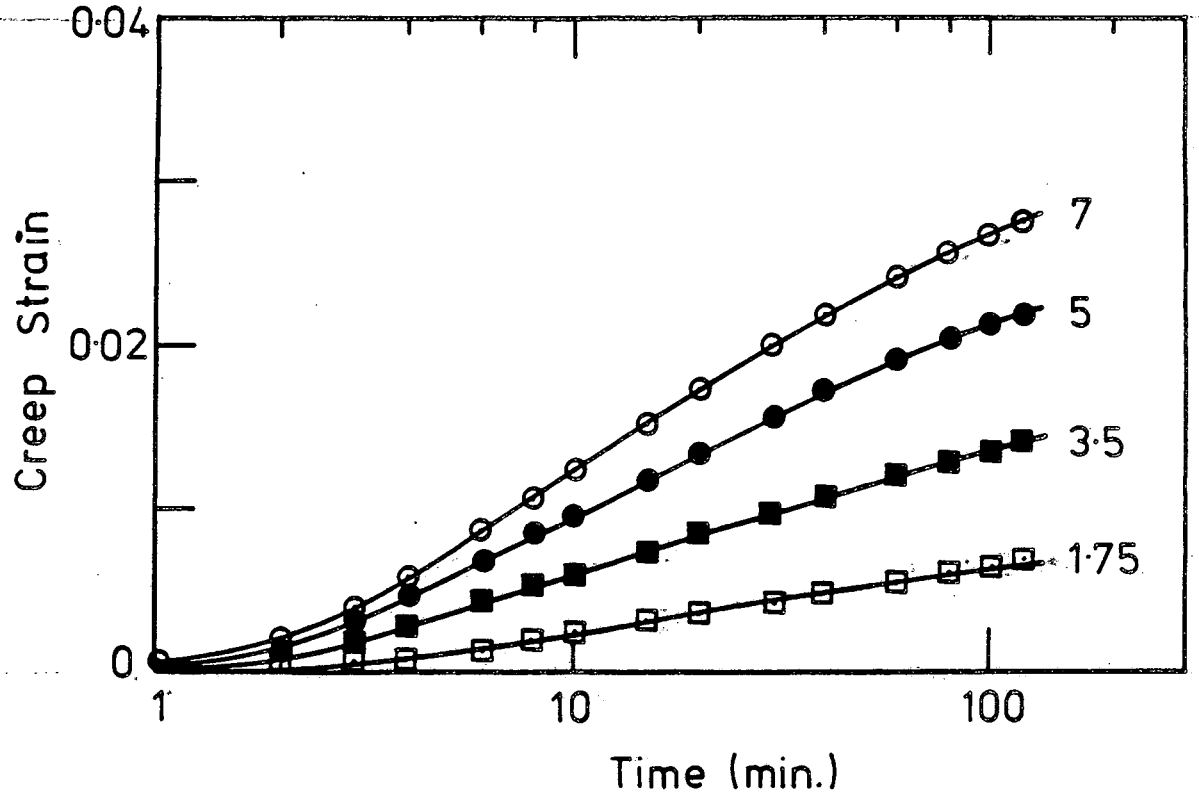

XBL 8612-4906

Fig. 4

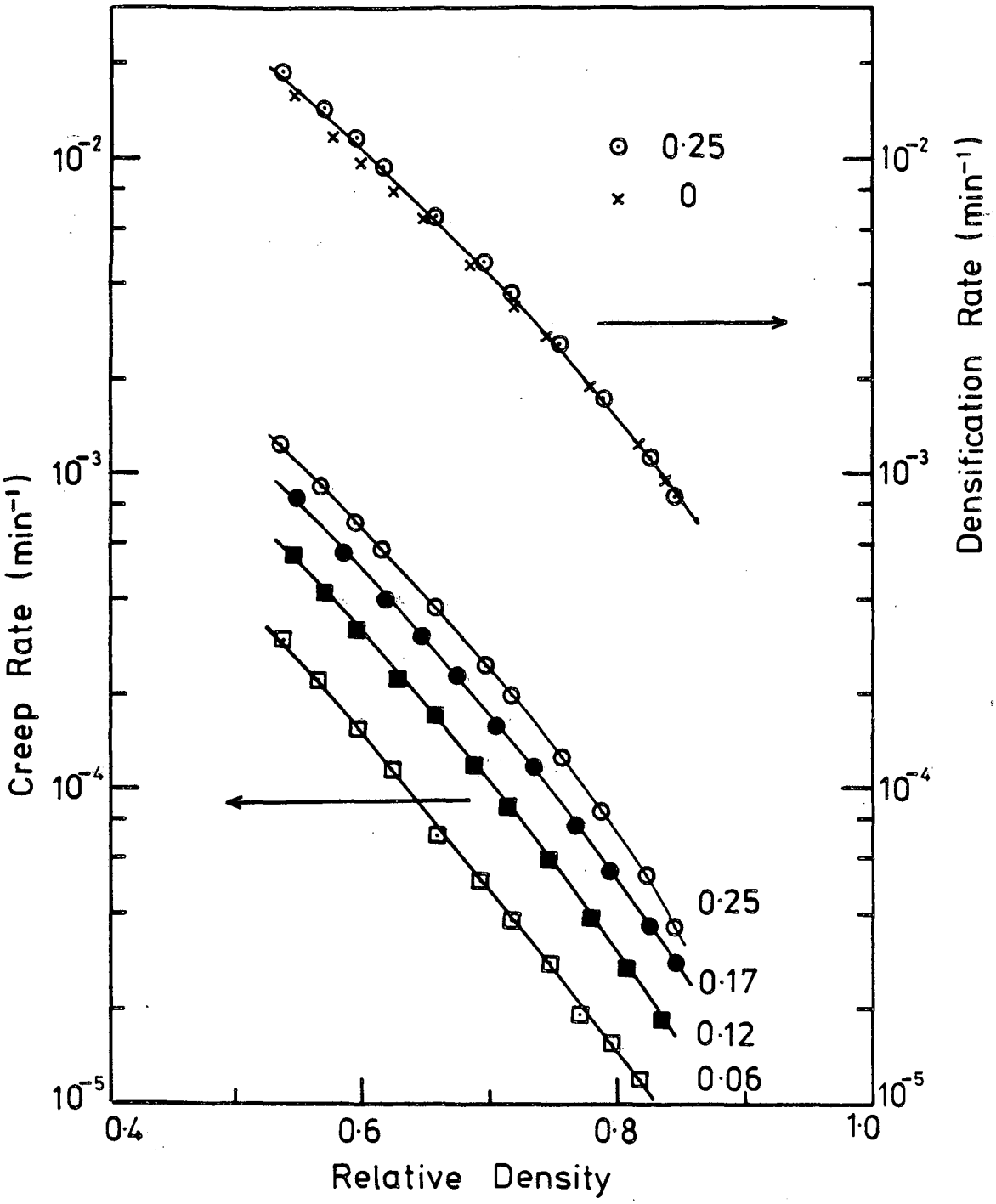

XBL 8612-4905

Fig. 5

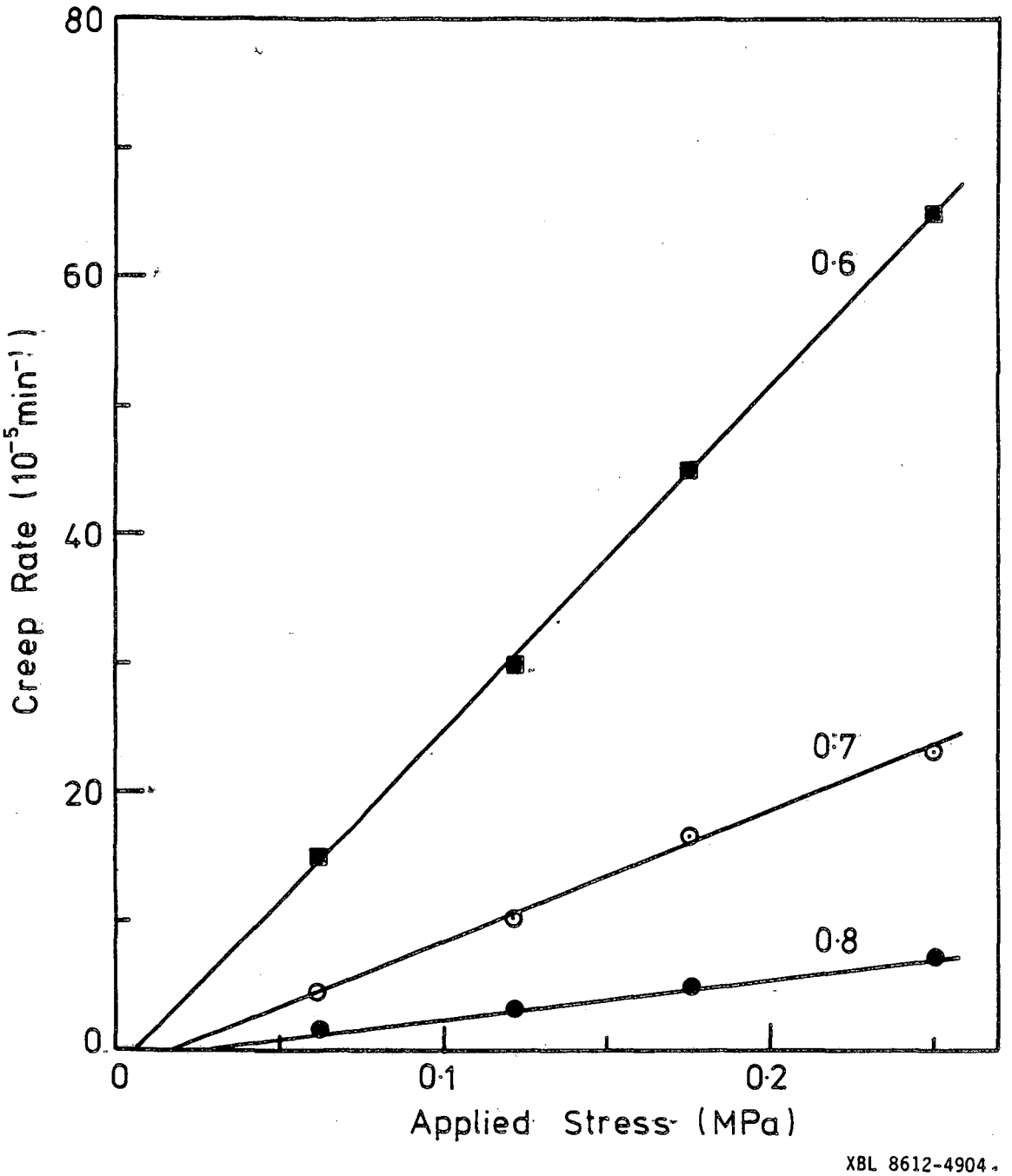
80
60
40
20
0
Creep Rate (10^{-5}min^{-1})
0·6
0·7
0·8
0
0·1
0·2
Applied Stress (MPa)
XBL 8612-4904

Fig. 6

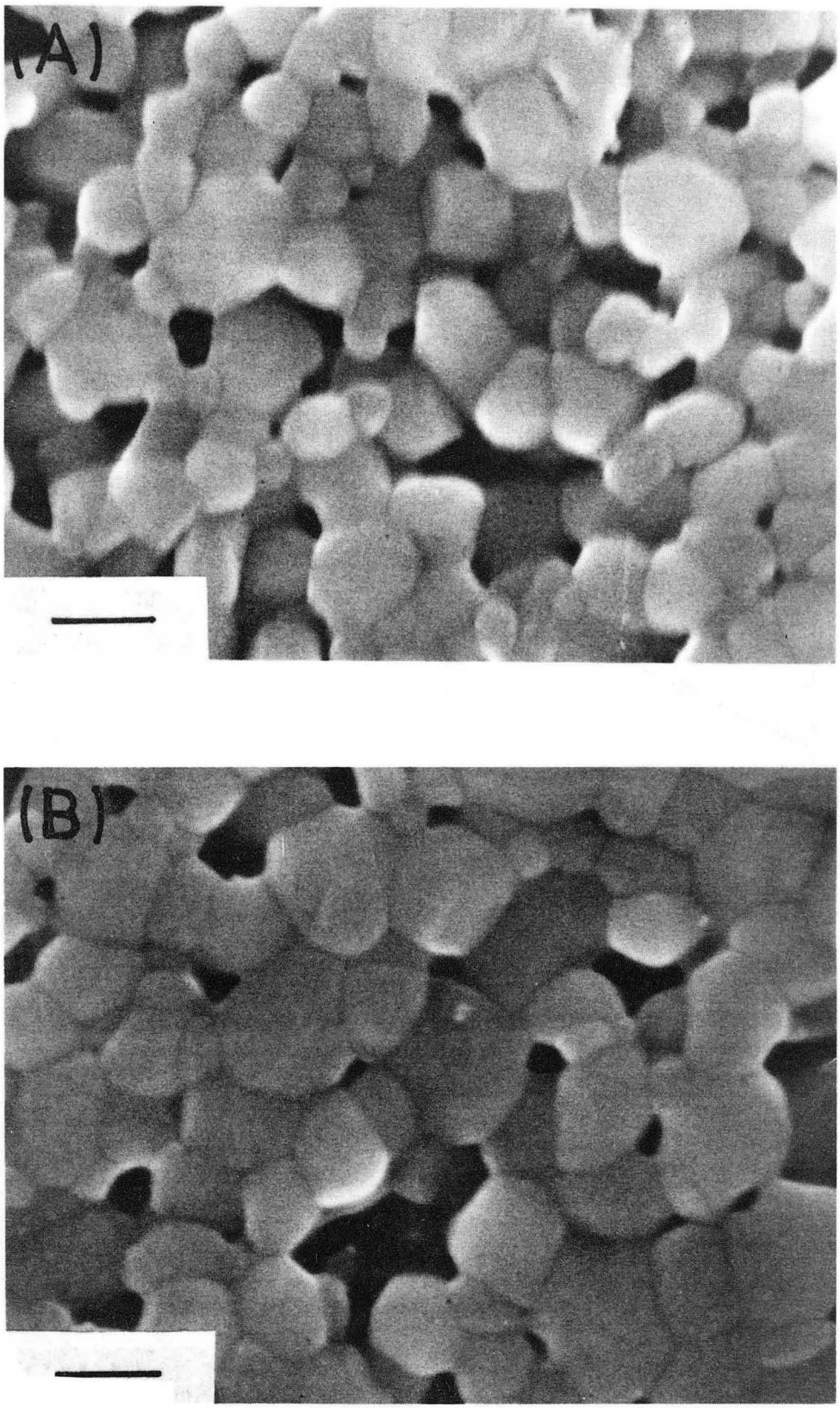

Fig. 7

XBB 860-10316

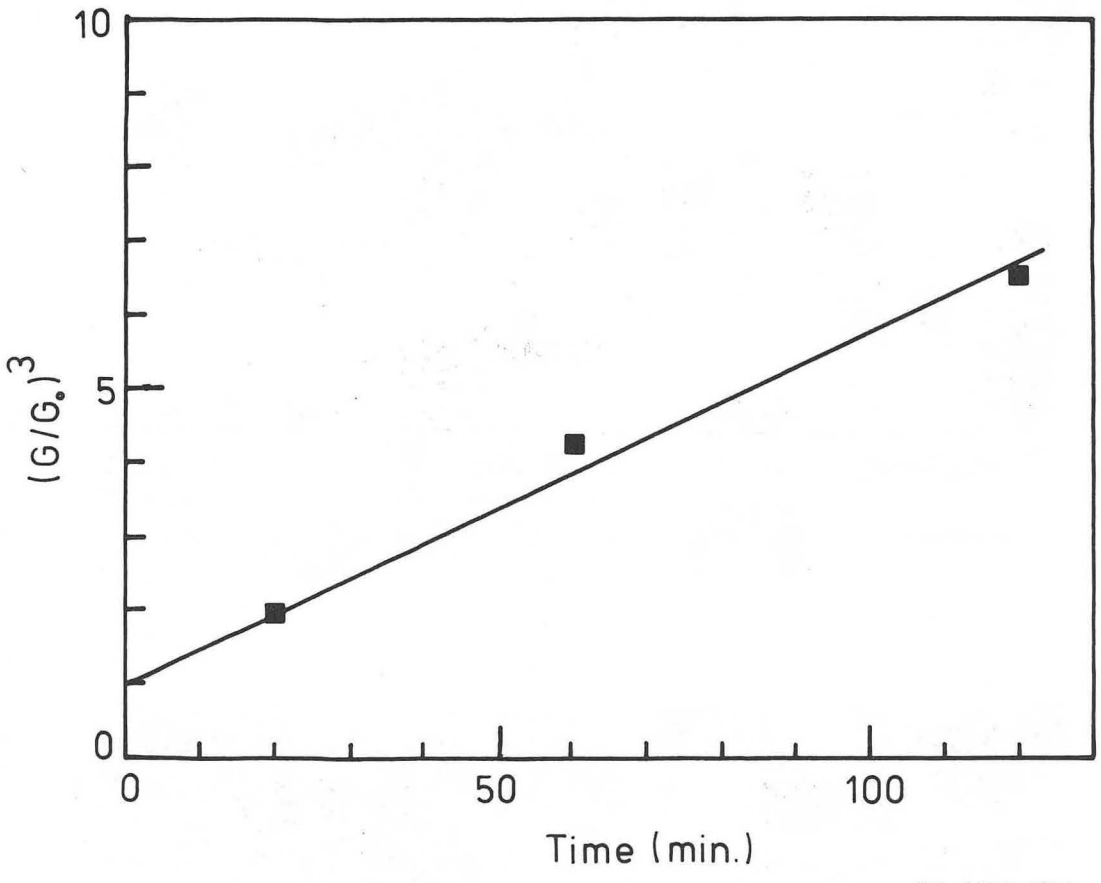

XBL 8612-4903

Fig. 8

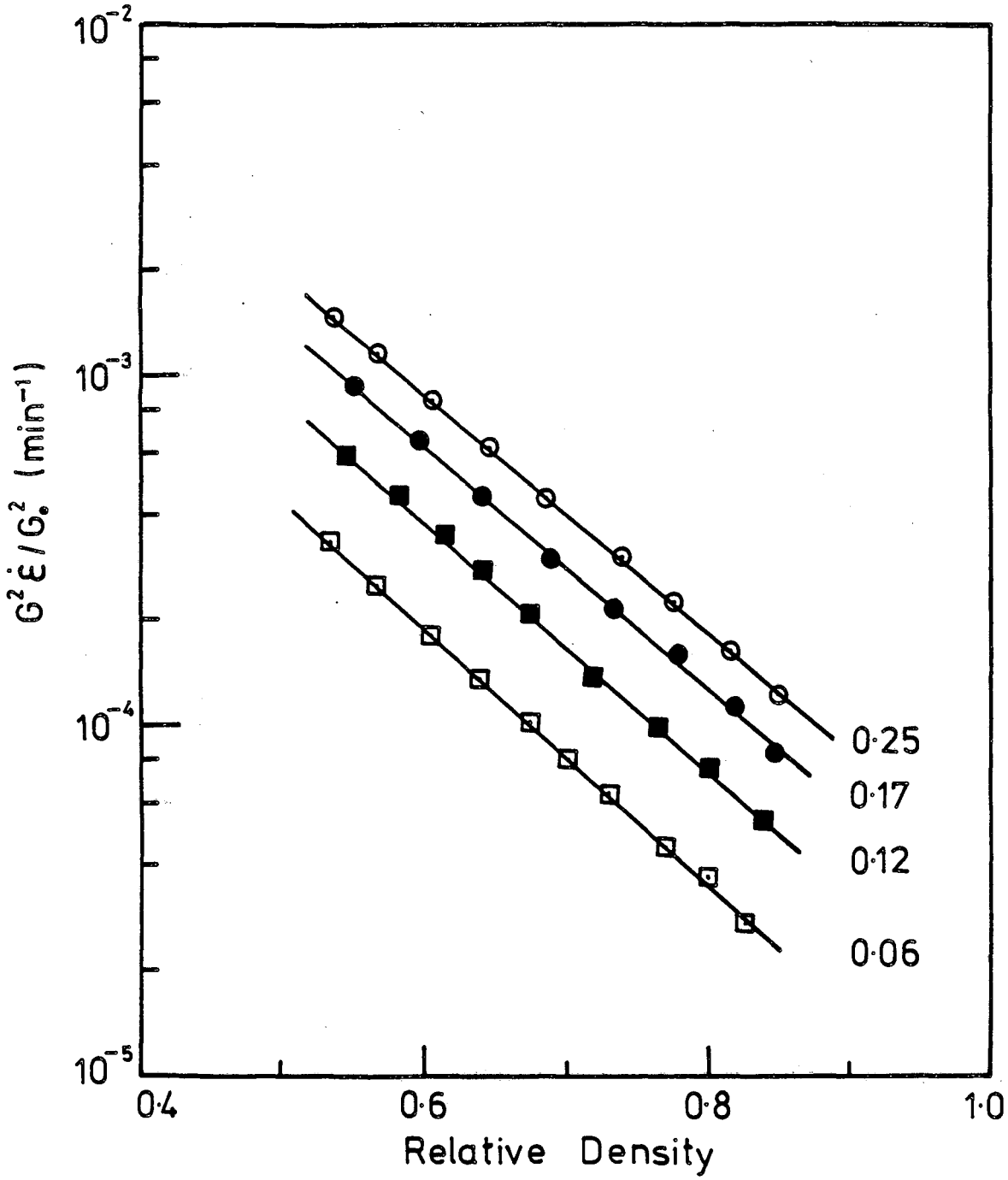
10^{-2}
10^{-3}
10^{-4}
10^{-5}
$G^2\dot{\varepsilon}/G_e^2$ (min^{-1})
0·4
0·6
0·8
1·0
Relative Density
0·25
0·17
0·12
0·06
XBL 8612-4902

Fig. 9

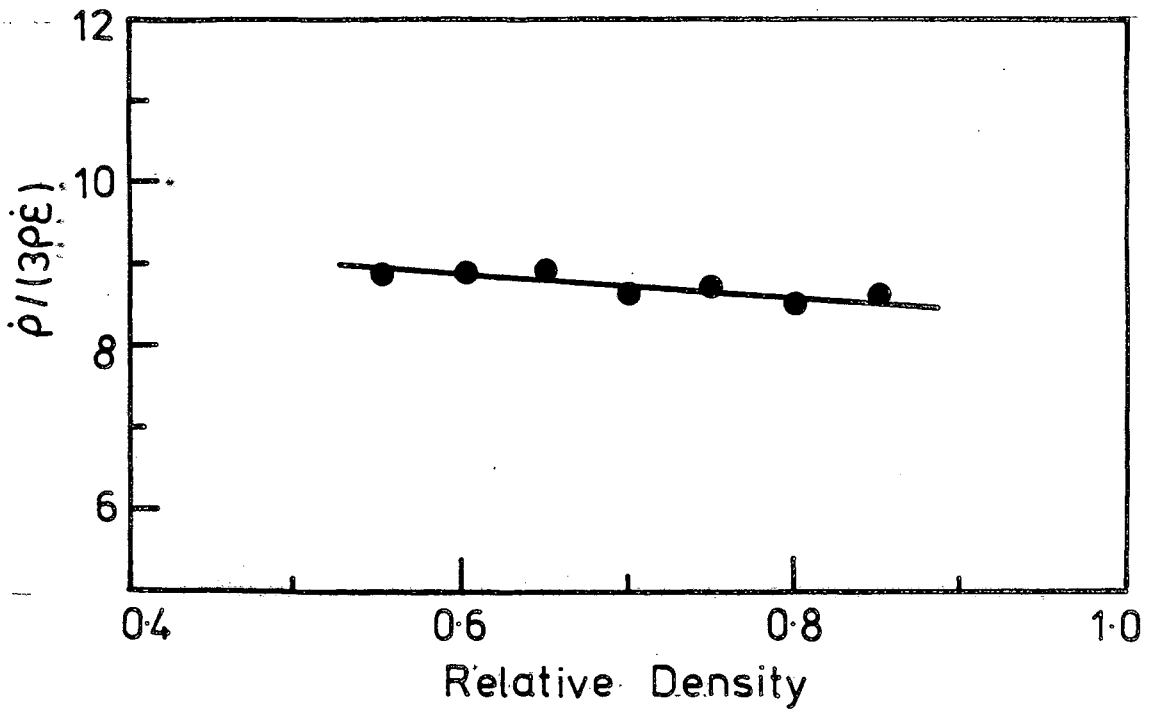

XBL 8612-4901

Fig. 10

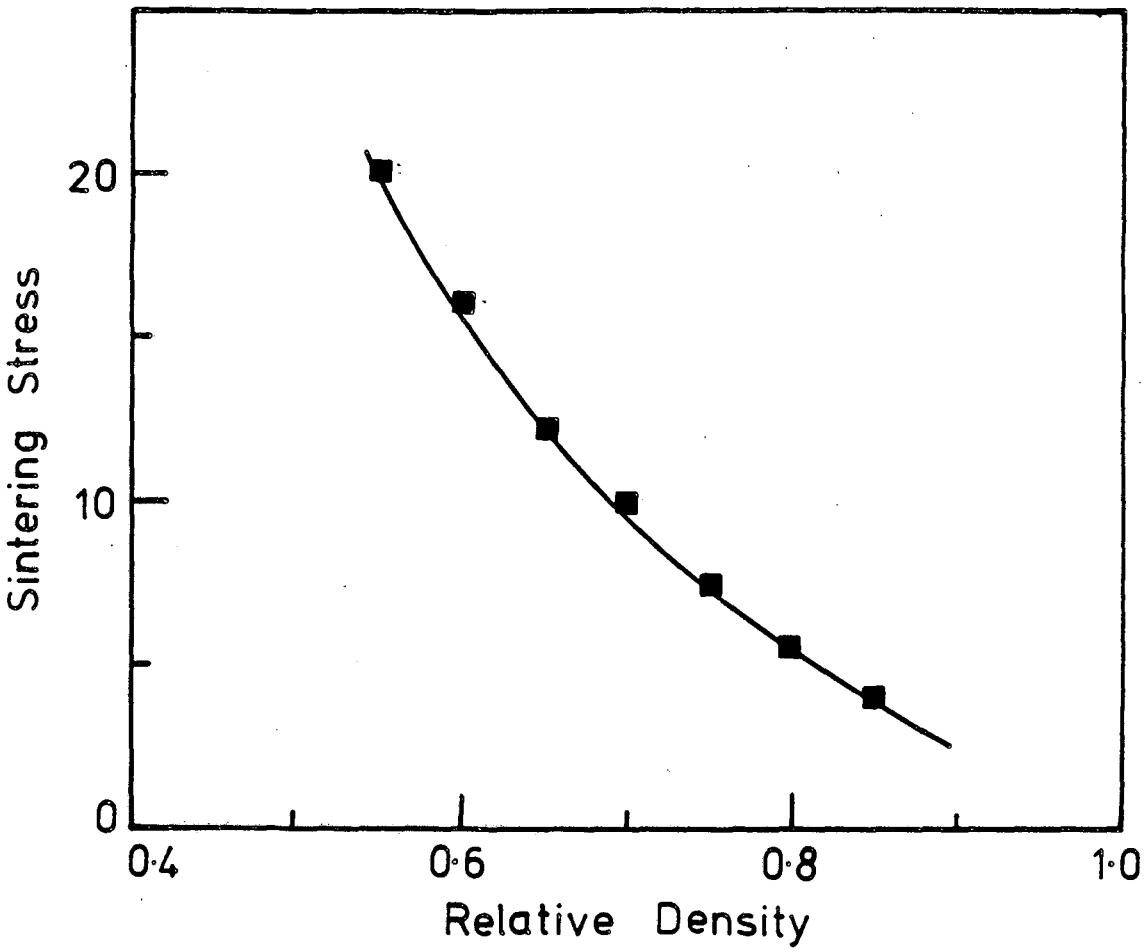

XBL 8612-4900

Fig. 11

This report was done with support from the Department of Energy. Any conclusions or opinions expressed in this report represent solely those of the author(s) and not necessarily those of The Regents of the University of California, the Lawrence Berkeley Laboratory or the Department of Energy.

Reference to a company or product name does not imply approval or recommendation of the product by the University of California or the U.S. Department of Energy to the exclusion of others that may be suitable.

LAWRENCE BERKELEY LABORATORY
TECHNICAL INFORMATION DEPARTMENT
UNIVERSITY OF CALIFORNIA
BERKELEY, CALIFORNIA 94720